

$K \rightarrow \pi\pi\pi\gamma$ in Chiral Perturbation Theory***G. D'Ambrosio¹, G. Ecker², G. Isidori³ and H. Neufeld²**

¹) INFN, Sezione di Napoli
Dipartimento di Scienze Fisiche, Università di Napoli
I-80125 Napoli, Italy

²) Institut für Theoretische Physik, Universität Wien
Boltzmannngasse 5, A-1090 Wien, Austria

³) INFN, Laboratori Nazionali di Frascati
P.O. Box 13, I-00044 Frascati, Italy

Abstract

We present a complete analysis of $K \rightarrow 3\pi\gamma$ decays to $\mathcal{O}(p^4)$ in the low-energy expansion of the Standard Model. We employ the notion of “generalized bremsstrahlung” to take full advantage of experimental information on the corresponding non-radiative $K \rightarrow 3\pi$ decays.

* Work supported in part by HCM, EEC-Contract No. CHRX-CT920026 (EURODAΦNE) and by FWF (Austria), Project Nos. P09505-PHY, P10876-PHY

1 Introduction

The present experimental status of $K \rightarrow 3\pi\gamma$ decays is rather meager. So far, only the two channels with a charged kaon in the initial state have been detected experimentally with very low statistics [1, 2, 3]. None of the decay modes of a neutral kaon have been seen.

This unsatisfactory experimental situation will change soon, especially after the completion of the e^+e^- collider DAΦNE in Frascati. In this Φ -factory one expects [4] a total yield of $7.5 \cdot 10^9$ $K_L K_S$ pairs and $1.1 \cdot 10^{10}$ $K^+ K^-$ pairs per year. For up-to-date information on the future prospects of kaon physics we refer to Ref. [5].

With a sufficient number of events, what can one learn from a study of those decays? The appropriate framework for such an investigation is chiral perturbation theory [6] (CHPT). To lowest order in an expansion in momenta and meson masses, the radiative decays are completely determined [7] by the non-radiative amplitudes for $K \rightarrow 3\pi$. At next-to-leading order, a full-fledged CHPT calculation of nonleptonic weak amplitudes of $\mathcal{O}(p^4)$ is required (cf., e.g., Ref. [8]). Among other ingredients to be discussed in Sec. 2, important components are the one-loop amplitudes with a single vertex from the lowest-order nonleptonic weak Lagrangian $\mathcal{L}_2^{|\Delta S|=1}$ and tree-level amplitudes due to the corresponding Lagrangian $\mathcal{L}_4^{|\Delta S|=1}$ of $\mathcal{O}(p^4)$.

There are three main issues we want to address:

- i. Bremsstrahlung completely determines the lowest-order amplitude, but it also contributes at next-to-leading order (and at higher orders as well). Is there a unique procedure to use all the available information on the non-radiative amplitudes to $\mathcal{O}(p^4)$, either from experiment or from theory? The answer is positive as shown previously for a general radiative four-meson process [7]. Here, we put the concept of “generalized bremsstrahlung” [7] to a practical test.
- ii. The nonleptonic weak Lagrangian of $\mathcal{O}(p^4)$ contains a number of low-energy constants [9, 10] that are little known at present. Can we expect to extract relevant information on those constants from $K \rightarrow 3\pi\gamma$ data?
- iii. More generally, can one make definite predictions for these radiative kaon decays within the Standard Model?

The outline of the paper is as follows. In Sec. 2, we set up the kinematics and discuss the low-energy expansion of $K \rightarrow 3\pi$ and $K \rightarrow 3\pi\gamma$ amplitudes up to $\mathcal{O}(p^4)$. We discuss the concept of generalized bremsstrahlung that takes full advantage of the available experimental information on the non-radiative amplitude in the form of a fourth-order polynomial in the momenta. In Sec. 3, we calculate the electric tree-level amplitude of $\mathcal{O}(p^4)$ in terms of the appropriate low-energy constants. We give a fairly complete list of experimentally accessible radiative kaon decays that depend on those weak constants of $\mathcal{O}(p^4)$. The calculation of the electric loop amplitude is deferred to an Appendix. To the same order in the chiral expansion, the magnetic amplitude is a pure tree-level amplitude that receives both direct (local) and reducible (nonlocal) contributions. These are put together in Sec. 4. Numerical results for rates and spectra of the four transitions occurring at $\mathcal{O}(p^4)$ are collected in Sec. 5. Some

conclusions are presented in Sec. 6. All relevant formulas for the one-loop amplitudes are contained in an Appendix, recapitulating and applying the results of Ref. [7].

2 Low-energy expansion

The kinematics of the decay $K(-p_4) \rightarrow \pi_1(p_1)\pi_2(p_2)\pi_3(p_3)\gamma(k)$ is specified by five scalar variables which we choose as

$$s = (p_1 + p_2)^2, \quad \nu = p_4(p_1 - p_2), \quad t_i = k \cdot p_i \quad (i = 1, \dots, 4) \quad (2.1)$$

with

$$\sum_{i=1}^4 p_i + k = 0, \quad \sum_{i=1}^4 t_i = 0.$$

Any three of the t_i together with s and ν form a set of independent variables.

The transition amplitude can be decomposed into an electric and a magnetic part:

$$A(K \rightarrow 3\pi\gamma) = e\varepsilon^\mu(k)(E_\mu + \varepsilon_{\mu\nu\rho\sigma}M^{\nu\rho\sigma}) \quad (2.2)$$

with

$$k^\mu E_\mu = 0, \quad \varepsilon_{\mu\nu\rho\sigma}k^\mu M^{\nu\rho\sigma} = 0.$$

To lowest order in the chiral expansion, the amplitudes for both radiative and non-radiative transitions are generated at tree level by the effective chiral Lagrangian of $\mathcal{O}(p^2)$,

$$\mathcal{L}_2 + \mathcal{L}_2^{|\Delta S|=1}. \quad (2.3)$$

The strong part has the well-known form [6]

$$\mathcal{L}_2 = \frac{F^2}{4} \langle D_\mu U D^\mu U^\dagger + 2\mathcal{B}\mathcal{M}(U + U^\dagger) \rangle \quad (2.4)$$

where $\langle \rangle$ denotes the trace in three-dimensional flavour space. F is the pion decay constant in the chiral limit ($F \simeq F_\pi = 92.4$ MeV), \mathcal{M} is the quark mass matrix and B is related to the quark condensate. The unitary 3×3 matrix field U incorporates the eight pseudoscalar meson fields. In the exponential parametrization,

$$U = \exp(i\sqrt{2}\Phi/F),$$

$$\Phi = \Phi^\dagger = \begin{pmatrix} \frac{\pi_0}{\sqrt{2}} + \frac{\eta}{\sqrt{6}} & \pi^+ & K^+ \\ \pi^- & -\frac{\pi_0}{\sqrt{2}} + \frac{\eta}{\sqrt{6}} & K^0 \\ K^- & \bar{K}^0 & -\frac{2\eta}{\sqrt{6}} \end{pmatrix}, \quad (2.5)$$

with $K_L = K_2^0 = (K^0 + \bar{K}^0)/\sqrt{2}$ and $K_S = K_1^0 = i(K^0 - \bar{K}^0)/\sqrt{2}$ in the limit of CP conservation. For the processes under consideration, the covariant derivative $D_\mu U$ can be restricted to

$$D_\mu U = \partial_\mu U + ieA_\mu[Q, U]$$

with the photon field A_μ and the quark charge matrix Q .

The weak $|\Delta S| = 1$ Lagrangian in (2.3) can be written in the form (our notation and conventions are those of Ref. [8])

$$\mathcal{L}_2^{|\Delta S|=1} = G_8 F^4 \langle \lambda L_\mu L^\mu \rangle + G_{27} F^4 \left(L_{\mu 23} L_{11}^\mu + \frac{2}{3} L_{\mu 21} L_{13}^\mu \right) + \text{h.c.} , \quad (2.6)$$

$$\lambda = \frac{1}{2}(\lambda_6 - i\lambda_7) , \quad L_\mu = iU^\dagger D_\mu U .$$

The coupling constants G_8 , G_{27} in (2.6) measure the strength of the octet and the 27-plet part, respectively, of the strangeness changing weak interactions. From $K \rightarrow \pi\pi$ decays one finds

$$|G_8| \simeq 9 \cdot 10^{-6} \text{ GeV}^{-2} , \quad G_{27}/G_8 \simeq 1/18 . \quad (2.7)$$

At lowest order, the magnetic amplitude $M^{\nu\rho\sigma}$ in (2.2) vanishes since there is no ε tensor in the Lagrangian (2.3). The electric amplitude, on the other hand, is completely determined by the corresponding non-radiative amplitude $A(s, \nu)$ via Low's theorem [11]:

$$\begin{aligned} E^\mu &= A(s, \nu) \Sigma^\mu \\ &+ 2 \frac{\partial A(s, \nu)}{\partial s} \Lambda_{12}^\mu + \frac{\partial A(s, \nu)}{\partial \nu} (\Lambda_{14}^\mu - \Lambda_{24}^\mu) \\ &+ \mathcal{O}(k) \end{aligned} \quad (2.8)$$

with (the meson charges in units of e are denoted q_i , with $\sum_{i=1}^4 q_i = 0$)

$$\begin{aligned} \Sigma^\mu &= \sum_{i=1}^4 \frac{q_i p_i^\mu}{t_i} \\ \Lambda_{ij}^\mu &= \Lambda_{ji}^\mu = (q_i t_j - q_j t_i) D_{ij}^\mu \\ D_{ij}^\mu &= -D_{ji}^\mu = \frac{p_i^\mu}{t_i} - \frac{p_j^\mu}{t_j} . \end{aligned} \quad (2.9)$$

Since there are no terms of $\mathcal{O}(k)$ at lowest order in the chiral expansion, the leading-order electric amplitude is completely determined by the explicit terms in (2.8) usually called ‘‘internal bremsstrahlung’’.

At next-to-leading order, $\mathcal{O}(p^4)$, the situation is much more complicated. A nonleptonic weak amplitude of $\mathcal{O}(p^4)$ receives in general four types of contributions [8]:

- i. Tree-level amplitudes from the effective chiral Lagrangian $\mathcal{L}_4^{|\Delta S|=1}$ of $\mathcal{O}(p^4)$ with the proper octet and 27-plet transformation properties.
- ii. One-loop amplitudes from diagrams with a single vertex from $\mathcal{L}_2^{|\Delta S|=1}$ in the loop.
- iii. Reducible tree-level amplitudes with a single vertex from $\mathcal{L}_2^{|\Delta S|=1}$ and with a single vertex either from the strong Lagrangian \mathcal{L}_4 or from the anomalous Wess-Zumino-Witten Lagrangian [12].

- iv. Reducible one-loop amplitudes, consisting of a strong loop diagram connected to a vertex of $\mathcal{L}_2^{|\Delta S|=1}$ by a single meson line. A typical diagram of this type contains an external $K - \pi$ or $K - \eta$ transition, possibly with an additional photon (generalized “pole diagrams”). The calculation of such diagrams is simplified by a rediagonalization of the kinetic and mass terms of $\mathcal{L}_2 + \mathcal{L}_2^{|\Delta S|=1}$ (“weak rotation” [13]).

For the decays $K \rightarrow 3\pi\gamma$, all four mechanisms are relevant. Most of them also appear in the non-radiative amplitudes. Via Low’s theorem (2.8), the non-radiative amplitude of $\mathcal{O}(p^4)$ will contribute to the electric part of the radiative amplitude. Unlike at lowest order, this is however not the whole story at $\mathcal{O}(p^4)$. The question then is how to use in an optimal way the amplitude $A(s, \nu)$ of $\mathcal{O}(p^4)$, either from theory or from experiment, for calculating the radiative electric amplitude E^μ of the same order.

In a recent paper [7], we have presented the general theoretical framework for the treatment of radiative four-meson amplitudes like $K \rightarrow 3\pi\gamma$. The essential point is the concept of “generalized bremsstrahlung”,

$$E^\mu = E_{\text{GB}}^\mu + \mathcal{O}(k) , \quad (2.10)$$

where E_{GB}^μ is defined in terms of the non-radiative amplitude $A(s, \nu)$ [7]:

$$\begin{aligned} E_{\text{GB}}^\mu &= A(s, \nu)\Sigma^\mu + 2\frac{\partial A(s, \nu)}{\partial s}\Lambda_{12}^\mu + \frac{\partial A(s, \nu)}{\partial \nu}(\Lambda_{14}^\mu - \Lambda_{24}^\mu) \\ &+ 2\frac{\partial^2 A(s, \nu)}{\partial s^2}(t_1 + t_2)\Lambda_{12}^\mu + \frac{1}{2}\frac{\partial^2 A(s, \nu)}{\partial \nu^2}[(t_1 - t_2)(\Lambda_{14}^\mu - \Lambda_{24}^\mu) - t_3 t_4 \Sigma^\mu] \\ &+ 2\frac{\partial^2 A(s, \nu)}{\partial s \partial \nu}[t_2 \Lambda_{14}^\mu - t_1 \Lambda_{24}^\mu] . \end{aligned} \quad (2.11)$$

Referring to Ref. [7] for a more thorough exposition, we concentrate here on the practical advantages of generalized bremsstrahlung. Many of the terms in the above list of four mechanisms appear in both the radiative and the non-radiative amplitudes and are therefore automatically included in E_{GB}^μ . This is in particular true for most of the renormalization parts that are trivially carried over from $A(s, \nu)$ to E^μ , but also for many of the so-called reducible contributions (items iii and iv in the above list). For instance, all the weak low-energy constants N_i [10] contributing to both $K \rightarrow 3\pi$ and $K \rightarrow 3\pi\gamma$ are completely taken into account by E_{GB}^μ . Therefore, only the genuine radiative low-energy constants N_{14}, \dots, N_{17} will show up in $E^\mu - E_{\text{GB}}^\mu$.

In the following we use the experimental $K \rightarrow 3\pi$ amplitudes to derive E_{GB}^μ . If we had limited ourselves to an analysis at the center of the Dalitz plot of $K \rightarrow 3\pi$ data [14, 15, 16] or just to linear slopes [17], there would have been no need to extend (2.8) to (2.11). However, the quadratic slopes are observed and the $K \rightarrow 3\pi$ amplitudes are written as polynomials of second order in s and ν [18, 19, 20] to fit the experimental data. The second derivatives in (2.11) are thus needed to take advantage of all the experimental information available from $K \rightarrow 3\pi$. The (electric) direct emission term $E^\mu - E_{\text{GB}}^\mu$ is then a genuine radiative part of the amplitude not related to the non-radiative transition.

In the numerical analysis we have used the following parametrization of the $K \rightarrow 3\pi$ amplitudes [20, 21]:

$$\begin{aligned}
A(K^+ \rightarrow \pi^0 \pi^0 \pi^+) &= a_c(1 + i\alpha_0 - i\alpha'_0 Y) - [b_c(1 + i\beta_0) - b_2(1 + i\delta_0)]Y \\
&\quad + c_c(Y^2 + X^2/3) - (d_c - d_2)(Y^2 - X^2/3) , \\
A(K^+ \rightarrow \pi^+ \pi^+ \pi^-) &= 2a_c(1 + i\alpha_0 + i\alpha'_0 Y/2) + [b_c(1 + i\beta_0) + b_2(1 + i\delta_0)]Y \\
&\quad + 2c_c(Y^2 + X^2/3) + (d_c + d_2)(Y^2 - X^2/3) , \\
A(K_L \rightarrow \pi^+ \pi^- \pi^0) &= a_n(1 + i\alpha_0 - i\alpha'_0 Y) - b_n(1 + i\beta_0)Y \\
&\quad + c_n(Y^2 + X^2/3) - d_n(Y^2 - X^2/3) , \\
A(K_S \rightarrow \pi^+ \pi^- \pi^0) &= -2i[b_2(1 + i\delta_0) - 2d_2 Y]X/3 ,
\end{aligned} \tag{2.12}$$

with

$$X = 2\nu/M_{\pi^+}^2 , \quad Y = (s - s_0)/M_{\pi^+}^2 , \quad s_0 = \sum_{i=1}^4 M_i^2/3 . \tag{2.13}$$

The numerical values for a_c , b_c , etc. (in units of 10^{-8}) are given by [19, 21]:

$$\begin{aligned}
a_c &= -95.39 \pm 0.40 , & a_n &= 84.35 \pm 0.57 , \\
b_c &= 24.47 \pm 0.34 , & b_n &= -28.11 \pm 0.49 , \\
c_c &= 0.68 \pm 0.17 , & c_n &= -0.05 \pm 0.22 , \\
d_c &= -1.63 \pm 0.34 , & d_n &= 1.27 \pm 0.45 , \\
b_2 &= -3.91 \pm 0.40 , & d_2 &= 0.21 \pm 0.51 .
\end{aligned} \tag{2.14}$$

For the phases associated with the absorptive parts in (2.12) we use the lowest-order CHPT predictions $\alpha_0 = 0.13$, $\alpha'_0 = -0.12$ and $\beta_0 = -\delta_0 = 0.047$ [20].

The decomposition (2.12) is based on isospin symmetry. Moreover, the numerical values in (2.14) have been obtained by a fit [19] where for simplicity the imaginary parts were set to zero. Present data on $K \rightarrow 3\pi$ are too poor¹ (especially in the K_S channel) both to relax the assumption of isospin conservation and to be sensitive to the small imaginary parts. As a consequence, our numerical predictions for the generalized bremsstrahlung amplitudes in $K \rightarrow 3\pi\gamma$ are affected by systematic errors and must be considered as preliminary. A new detailed analysis should be performed when complete and accurate $K \rightarrow 3\pi$ data will be available.

In the next two sections we discuss separately the electric and the magnetic amplitudes for the various channels. To $\mathcal{O}(p^4)$, there are four non-vanishing transitions:

$$\begin{aligned}
K^+ &\rightarrow \pi^0 \pi^0 \pi^+ \gamma & K^+ &\rightarrow \pi^+ \pi^+ \pi^- \gamma \\
K_L &\rightarrow \pi^+ \pi^- \pi^0 \gamma & K_S &\rightarrow \pi^+ \pi^- \pi^0 \gamma .
\end{aligned}$$

We make the following simplifications for the calculation. The 27-plet part of the nonleptonic weak Lagrangian is not included in the calculation of direct emission amplitudes, i.e. in $(E^\mu - E_{\text{GB}}^\mu)$ and $M^{\nu\rho\sigma}$. This is an excellent approximation in view of the $\Delta I = 1/2$ rule. Moreover, in the loop diagrams we have only kept the dominant two-pion intermediate states. Since the loop amplitudes will turn out to be rather small anyway, this restriction is justified a posteriori. Finally, CP conservation will be assumed throughout the analysis.

¹ Note that we have not taken into account the very recent and accurate results of Serpukhov-167 [22] in the $K^+ \rightarrow \pi^0 \pi^0 \pi^+$ channel.

3 Electric amplitudes

To $\mathcal{O}(p^4)$, the electric amplitude can be written as

$$E^\mu = E_{\text{GB}}^\mu + E_{\text{counter}}^\mu + E_{\text{loop,subtracted}}^\mu . \quad (3.1)$$

Use of the generalized bremsstrahlung amplitude E_{GB}^μ greatly simplifies the calculation of both the tree-level and the loop part of (3.1). For instance, all the reducible contributions (items iii and iv in the list of Sec. 2) to the electric amplitude are automatically contained in E_{GB}^μ . This can be shown almost without any calculation by going back to the definition (2.11) of generalized bremsstrahlung. The only exception that needs some (tree-level) calculations are amplitudes proportional to the strong low-energy constant L_9 [6] with an external weak transition. Although there are strong radiative four-meson amplitudes proportional to L_9 , the explicit calculation shows that they do not contribute to $K \rightarrow 3\pi\gamma$ after a weak rotation.

Another consequence of using generalized bremsstrahlung in (3.1) is a much simpler form of E_{counter}^μ . All the low-energy constants appearing in both radiative and non-radiative amplitudes are already contained in E_{GB}^μ . Therefore, only the genuine radiative terms in the octet Lagrangian of $\mathcal{O}(p^4)$ [10]

$$\mathcal{L}_4^{|\Delta S|=1} = G_8 F^2 \sum_i N_i W_i + \text{h.c.} , \quad (3.2)$$

with dimensionless coupling constants N_i and octet operators W_i , contribute to E_{counter}^μ . In particular, going through the Lagrangian (3.2) one finds that only the four low-energy constants N_{14}, \dots, N_{17} can occur in E_{counter}^μ . The relevant parts of the Lagrangian (3.2) are listed below.

With $F_{\mu\nu} = \partial_\mu A_\nu - \partial_\nu A_\mu$ the electromagnetic field strength tensor, the explicit coupling for $K^+ \rightarrow \pi^0 \pi^0 \pi^+ \gamma$ is given by

$$- \frac{ieG_8}{F^2} (N_{14} - N_{15} - N_{16} - N_{17}) F_{\mu\nu} K^+ \pi^0 \partial^\mu \pi^0 \partial^\nu \pi^- . \quad (3.3)$$

The corresponding expression for $K^+ \rightarrow \pi^+ \pi^+ \pi^- \gamma$ reads

$$- \frac{4ieG_8}{F^2} (N_{14} - N_{15} - N_{16} - N_{17}) F_{\mu\nu} K^+ \pi^- \partial^\mu \pi^+ \partial^\nu \pi^- . \quad (3.4)$$

The decay $K_L \rightarrow \pi^+ \pi^- \pi^0 \gamma$ receives a contribution from

$$- \frac{ieG_8}{F^2} (N_{14} - N_{15} - N_{16} - N_{17}) F_{\mu\nu} K_L (\partial^\mu \pi^0 \pi^- \overleftrightarrow{\partial}^\nu \pi^+ - 2\pi^0 \partial^\mu \pi^+ \partial^\nu \pi^-) , \quad (3.5)$$

and $K_S \rightarrow \pi^+ \pi^- \pi^0 \gamma$ from

$$- \frac{eG_8}{F^2} [7(N_{14} - N_{16}) + 5(N_{15} + N_{17})] F_{\mu\nu} K_S \partial^\mu \pi^0 (\pi^- \partial^\nu \pi^+ + \pi^+ \partial^\nu \pi^-) . \quad (3.6)$$

In order to facilitate the comparison with other radiative kaon decays, we list in Table 1 the combinations of low-energy constants N_i governing the various experimentally accessible

Table 1: Kaon decay modes to which the coupling constants N_i contribute. For the 3π final states, only the single photon channels are listed. For the neutral modes, the letters L or S in brackets distinguish between K_L and K_S in the limit of CP conservation. γ^* denotes a lepton pair in the final state. If a decay mode appears more than once there are different Lorentz structures in the amplitude. The combinations with N_i^r are scale dependent compensating the scale dependence of the corresponding loop amplitude. The other combinations are scale independent.

π	2π	3π	N_i
$\pi^+\gamma^*$	$\pi^+\pi^0\gamma^*$		$N_{14}^r - N_{15}^r$
$\pi^0\gamma^* (S)$	$\pi^0\pi^0\gamma^* (L)$		$2N_{14}^r + N_{15}^r$
$\pi^+\gamma\gamma$	$\pi^+\pi^0\gamma\gamma$		$N_{14} - N_{15} - 2N_{18}$
	$\pi^+\pi^-\gamma\gamma (S)$		"
	$\pi^+\pi^0\gamma$	$\pi^+\pi^+\pi^-\gamma$	$N_{14} - N_{15} - N_{16} - N_{17}$
	$\pi^+\pi^-\gamma (S)$	$\pi^+\pi^0\pi^0\gamma$	"
		$\pi^+\pi^-\pi^0\gamma (L)$	"
		$\pi^+\pi^-\pi^0\gamma (S)$	$7(N_{14}^r - N_{16}^r) + 5(N_{15}^r + N_{17}^r)$
	$\pi^+\pi^-\gamma^* (L)$		$N_{14}^r - N_{15}^r - 3(N_{16}^r - N_{17}^r)$
	$\pi^+\pi^-\gamma^* (S)$		$N_{14}^r - N_{15}^r - 3(N_{16}^r + N_{17}^r)$
	$\pi^+\pi^0\gamma^*$		$N_{14}^r + 2N_{15}^r - 3(N_{16}^r - N_{17}^r)$
	$\pi^+\pi^-\gamma (L)$	$\pi^+\pi^-\pi^0\gamma (S)$	$N_{29} + N_{31}$
		$\pi^+\pi^+\pi^-\gamma$	"
	$\pi^+\pi^0\gamma$	$\pi^+\pi^0\pi^0\gamma$	$3N_{29} - N_{30}$
		$\pi^+\pi^-\pi^0\gamma (S)$	$5N_{29} - N_{30} + 2N_{31}$
		$\pi^+\pi^-\pi^0\gamma (L)$	$6N_{28} + 3N_{29} - 5N_{30}$

channels. This Table is a slightly extended version of the one appearing in Ref. [8]. As one can see from the Table, the specific combination of coupling constants $N_{14} - N_{15} - N_{16} - N_{17}$ occurs also in the amplitudes for $K^+ \rightarrow \pi^+\pi^0\gamma$ and $K_S \rightarrow \pi^+\pi^-\gamma$. On the other hand, $7(N_{14}^r - N_{16}^r) + 5(N_{15}^r + N_{17}^r)$ is a characteristic combination² for $K_S \rightarrow \pi^+\pi^-\pi^0\gamma$ only.

Both combinations are not yet known phenomenologically. To get a feeling for the typical size of these couplings one may appeal to the factorization model that predicts [10]

$$[N_{14} - N_{15} - N_{16} - N_{17}]^{\text{FM}} = -k_f \frac{F_\pi^2}{2M_V^2} = -7 \cdot 10^{-3} k_f, \quad (3.7)$$

$$[7(N_{14} - N_{16}) + 5(N_{15} + N_{17})]^{\text{FM}} = 41k_f \frac{F_\pi^2}{2M_V^2}, \quad (3.8)$$

where k_f is a fudge factor which naive factorization sets equal to one. Note the potentially large counterterm amplitude in $K_S \rightarrow \pi^+\pi^-\pi^0\gamma$. Table 1 also indicates that the combination $N_{14} - N_{15} - N_{16} - N_{17}$ is scale independent while $7(N_{14}^r - N_{16}^r) + 5(N_{15}^r + N_{17}^r)$ is not. Consequently, the loop amplitudes are all finite for $K^+ \rightarrow \pi^0\pi^0\pi^+\gamma$, $K^+ \rightarrow \pi^+\pi^+\pi^-\gamma$ and

²We remind the reader that N_{17} is scale independent [10].

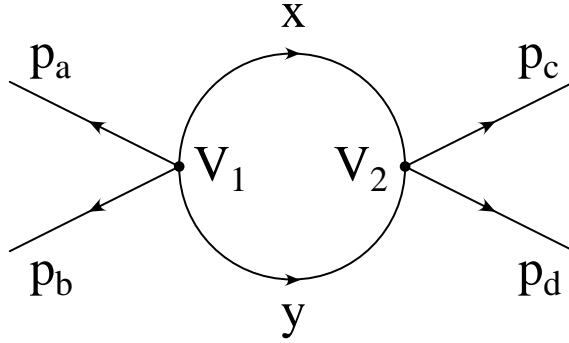


Figure 1: One-loop diagram for a four-meson transition. For the radiative amplitude, the photon must be appended to every charged meson line and to every vertex with at least two charged fields. For the case of $K \rightarrow 3\pi(\gamma)$, $-p_a = -p_4$ is the kaon momentum, the other three being the pion momenta. The weak (strong) vertex V_1 (V_2) is defined in Eq. (A.1), with the appropriate coefficients for the various diagrams given in Table 6.

$K_L \rightarrow \pi^+\pi^-\pi^0\gamma$, but divergent for $K_S \rightarrow \pi^+\pi^-\pi^0\gamma$. This divergence is renormalized by the counterterm combination $7(N_{14} - N_{16}) + 5(N_{15} + N_{17})$. In the limit where G_{27} is set to zero, the two-pion loop does not contribute to the K_S decay. Since we have not included the other loop contributions that are numerically negligible, the amplitude of $\mathcal{O}(p^4)$ for the K_S decay is superficially scale dependent. We shall come back in Sec. 5 to investigate numerically the effect of this scale dependence.

Finally, the loop contributions to (3.1) have to be calculated. Once again, many contributions are already contained in E_{GB}^μ . The only type of diagram that has to be calculated explicitly is shown in Fig. 1 where a photon can be appended to all (charged) lines and vertices. In this diagram, V_1 is a weak vertex from $\mathcal{L}_2^{|\Delta S|=1}$ and V_2 is a strong vertex from \mathcal{L}_2 . Of course, such diagrams without a photon contribute also to the $K \rightarrow 3\pi$ amplitudes of $\mathcal{O}(p^4)$. In accordance with the definition of generalized bremsstrahlung in (2.11), the appropriate part has been subtracted from the radiative loop amplitude to obtain $E_{\text{loop,subtracted}}^\mu$ in the complete amplitude (3.1).

The calculation of the loop amplitudes is rather involved in the radiative case. We have given in Ref. [7] a compact expression for the radiative loop amplitude with general vertices V_1, V_2 of $\mathcal{O}(p^2)$. In an Appendix, we reproduce the main steps for arriving at the final amplitude, together with the relevant vertices for $K \rightarrow 3\pi\gamma$.

4 Magnetic amplitudes

The magnetic amplitude in (2.2) receives contributions from direct and reducible diagrams [23, 24] corresponding to type i and iii, respectively, in the classification of Sec. 2.

The direct parts (type i) are generated by the operators W_{28}, \dots, W_{31} in (3.2). Their contribution to $K^+ \rightarrow \pi^0\pi^0\pi^+\gamma$ is given by

$$-\frac{eG_8}{F^2}(3N_{29} - N_{30})\tilde{F}_{\mu\nu}\partial^\mu K^+\partial^\nu\pi^-\pi^0\pi^0, \quad (4.1)$$

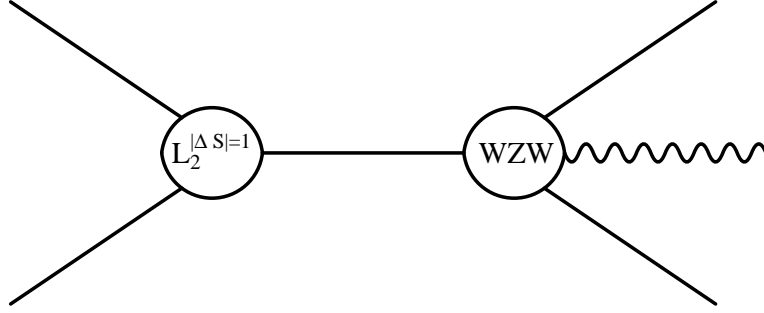


Figure 2: Reducible diagram contributing to the magnetic amplitude at $\mathcal{O}(p^4)$. A weak cubic vertex of $\mathcal{O}(p^2)$ and an anomalous vertex with three mesons and a photon are connected by a single meson line.

where $\tilde{F}_{\mu\nu} = \varepsilon_{\mu\nu\rho\sigma} F^{\rho\sigma}$ ($\varepsilon_{0123} = +1$). The corresponding expression for $K^+ \rightarrow \pi^+\pi^+\pi^-\gamma$ reads

$$- \frac{4eG_8}{F^2} (N_{29} + N_{31}) \tilde{F}_{\mu\nu} \partial^\mu K^+ \partial^\nu \pi^+ \pi^- \pi^- . \quad (4.2)$$

The decay $K_L \rightarrow \pi^+\pi^-\pi^0\gamma$ receives a contribution from

$$- \frac{2eG_8}{F^2} (6N_{28} + 3N_{29} - 5N_{30}) \tilde{F}_{\mu\nu} \partial^\mu K_L \partial^\nu \pi^0 \pi^- \pi^+ , \quad (4.3)$$

and $K_S \rightarrow \pi^+\pi^-\pi^0\gamma$ from

$$\frac{2ieG_8}{F^2} \tilde{F}_{\mu\nu} K_S [(5N_{29} - N_{30} + 2N_{31}) \partial^\mu \pi^0 \pi^- \overleftrightarrow{\partial}^\nu \pi^+ - 2(N_{29} + N_{31}) \pi^0 \partial^\mu \pi^+ \partial^\nu \pi^-] . \quad (4.4)$$

Following the theoretical arguments given in [25], the coupling constants in the anomalous parity sector of $\mathcal{O}(p^4)$ can be estimated as

$$\begin{aligned} N_{28}^{\text{an}} &= \frac{a_1}{8\pi^2} , & N_{29}^{\text{an}} &= \frac{a_2}{32\pi^2} , \\ N_{30}^{\text{an}} &= \frac{3a_3}{16\pi^2} , & N_{31}^{\text{an}} &= \frac{a_4}{16\pi^2} , \end{aligned} \quad (4.5)$$

where the dimensionless coefficients a_i are expected to be positive and of order one.

The second class of diagrams contributing to the magnetic amplitude are the reducible ones (type iii). These amplitudes are due to diagrams with a single meson line between a weak $|\Delta S| = 1$ vertex and an anomalous vertex from the Wess–Zumino–Witten (WZW) functional [12]. For $K \rightarrow 3\pi\gamma$, all such diagrams have the structure shown in Fig. 2: a weak cubic vertex and an anomalous vertex with three mesons and a photon.

In the case of $K^+ \rightarrow \pi^0\pi^0\pi^+\gamma$, there is only one reducible contribution at $\mathcal{O}(p^4)$: the kaon emits a neutral and a charged pion, where the π^+ subsequently makes an anomalous transition to $\pi^0\pi^+\gamma$,

$$K^+ \xrightarrow{\text{weak}} \pi^0 (\pi^+ \xrightarrow{\text{WZW}} \pi^0 \pi^+ \gamma) .$$

The corresponding amplitude is local because the $K^+ \rightarrow \pi^0\pi^+$ vertex vanishes on-shell (remember that we are setting $G_{27} = 0$ in direct emission amplitudes). Thus, the complete

magnetic amplitude (adding the direct term generated by (4.1)) takes the form

$$M^{\nu\rho\sigma}(K^+ \rightarrow \pi^0\pi^0\pi^+\gamma) = \frac{iG_8}{8\pi^2F^2}(3a_2 - 6a_3 - 2)k^\nu p_3^\rho p_4^\sigma . \quad (4.6)$$

There are two types of reducible diagrams contributing to $K^+ \rightarrow \pi^+\pi^+\pi^-\gamma$: the K^+ can make a weak transition into a real π^+ and a virtual π^0 (or η) which is then transformed into a $\pi^+\pi^-$ pair and a photon,

$$K^+ \xrightarrow{\text{weak}} \pi^+(\pi^0 \xrightarrow{\text{WZW}} \pi^+\pi^-\gamma) ,$$

$$K^+ \xrightarrow{\text{weak}} \pi^+(\eta \xrightarrow{\text{WZW}} \pi^+\pi^-\gamma) .$$

The total magnetic amplitude is now given by

$$\begin{aligned} M^{\nu\rho\sigma}(K^+ \rightarrow \pi^+\pi^+\pi^-\gamma) &= \frac{iG_8}{2\pi^2F^2}k^\nu p_3^\rho [(a_2 + 2a_4)p_4^\sigma \\ &\quad + (M_\eta^2 - M_K^2)\left(\frac{p_1^\sigma}{s_{24} - M_\eta^2} + \frac{p_2^\sigma}{s_{14} - M_\eta^2}\right)] , \end{aligned} \quad (4.7)$$

with

$$s_{14} = (p_1 + p_4)^2 = \nu + t_3 + (M_K^2 + 3M_\pi^2 - s)/2 ,$$

$$s_{24} = (p_2 + p_4)^2 = -\nu + t_3 + (M_K^2 + 3M_\pi^2 - s)/2 .$$

For $K_L \rightarrow \pi^+\pi^-\pi^0\gamma$ one may either contract the anomalous $K_L K_S \pi^0 \gamma$ vertex with the weak $K_S \pi^+ \pi^-$ vertex, or the weak $K_L \rightarrow \pi^+ \pi^-$ transition with the $\pi^+ \pi^- \pi^0 \gamma$ WZW vertex:

$$K_L \xrightarrow{\text{WZW}} \pi^0 \gamma (K_S \xrightarrow{\text{weak}} \pi^+ \pi^-) ,$$

$$K_L \xrightarrow{\text{weak}} \pi^+ (\pi^- \xrightarrow{\text{WZW}} \pi^- \pi^0 \gamma) ,$$

$$K_L \xrightarrow{\text{weak}} \pi^- (\pi^+ \xrightarrow{\text{WZW}} \pi^+ \pi^0 \gamma) .$$

The last two diagrams give again a local amplitude for a similar reason³ as for $K^+ \rightarrow \pi^0\pi^0\pi^+\gamma$ in (4.6). Together with the contribution from (4.3), we arrive at the magnetic amplitude

$$M^{\nu\rho\sigma}(K_L \rightarrow \pi^+\pi^-\pi^0\gamma) = \frac{iG_8}{8\pi^2F^2}[24a_1 + 3a_2 - 30a_3 - 2 - \frac{4(M_K^2 - M_\pi^2)}{s - M_K^2}]k^\nu p_3^\rho p_4^\sigma . \quad (4.8)$$

Finally, we turn to $K_S \rightarrow \pi^+\pi^-\pi^0\gamma$. In this case, the reducible diagrams have the following structure:

$$K_S \xrightarrow{\text{weak}} \pi^+ (\pi^- \xrightarrow{\text{WZW}} \pi^- \pi^0 \gamma) ,$$

$$K_S \xrightarrow{\text{weak}} \pi^- (\pi^+ \xrightarrow{\text{WZW}} \pi^+ \pi^0 \gamma) ,$$

$$K_S \xrightarrow{\text{weak}} \pi^0 (\pi^0 \xrightarrow{\text{WZW}} \pi^+ \pi^- \gamma) ,$$

$$K_S \xrightarrow{\text{weak}} \pi^0 (\eta \xrightarrow{\text{WZW}} \pi^+ \pi^- \gamma) .$$

³The on-shell amplitude for $K_L \rightarrow \pi^+\pi^-$ vanishes in the limit of CP conservation.

Combined with (4.4), we obtain

$$\begin{aligned}
M^{\nu\rho\sigma}(K_S \rightarrow \pi^+\pi^-\pi^0\gamma) &= \frac{G_8}{8\pi^2 F^2} k^\nu \{ (5a_2 - 6a_3 + 4a_4 - 2)(p_2 - p_1)^\rho p_3^\sigma \\
&+ 4(M_K^2 - M_\pi^2) \left(\frac{p_2^\rho}{s_{14} - M_\pi^2} - \frac{p_1^\rho}{s_{24} - M_\pi^2} \right) p_3^\sigma \\
&+ [-2a_2 - 4a_4 + \frac{4(M_K^2 - M_\pi^2)}{s_{34} - M_\pi^2} + \frac{4(M_\eta^2 - M_K^2)}{s_{34} - M_\eta^2}] p_1^\rho p_2^\sigma \} ,
\end{aligned} \tag{4.9}$$

where

$$s_{34} = (p_3 + p_4)^2 = s + 2(t_1 + t_2) .$$

5 Numerical results

Our numerical results for the various channels are displayed in Tables 2 – 5. The first column shows the photon energy range. In the second column, the contribution to the decay width generated by the generalized bremsstrahlung amplitude E_{GB} in (2.11) is listed, together with the corresponding errors due to the uncertainties of the $K \rightarrow 3\pi$ parameters in (2.14). The next column shows the relative change of the result if only the Low amplitude (2.8) is used instead of E_{GB} . In the fourth column we see the effect of adding the electric counterterms (using $k_f = 1$ in (3.7) and (3.8)) and the residual pion-loop contributions $E_{\text{loop,subtracted}}$ in (3.1). Γ_{M} in the next column denotes the contribution to the decay width from the magnetic amplitudes (for $a_i = 1$); there is no interference between electric and magnetic amplitudes as long as the phase space integration is performed “symmetrically”.

For the branching ratios in the last column we distinguish between the three channels where the leading-order amplitude is not suppressed and the decay $K_S \rightarrow \pi^+\pi^-\pi^0\gamma$ with a suppressed bremsstrahlung amplitude. In the first group of transitions, the dominant $\mathcal{O}(E_\gamma)$ effect is given by the difference $\Gamma_{\text{GB}} - \Gamma_{\text{Low}}$. This deviation from Low’s theorem, i.e. from a pure QED prediction, could possibly be observed in the near future. In the above channels, the residual pion-loop contribution suffers from relatively large theoretical uncertainties: the smallness of phase space amplifies isospin-breaking effects generated by the mass difference $M_{\pi^0} - M_{\pi^\pm}$. However, the effect of $E_{\text{loop,subtracted}}$ is always so small that it can hardly be detected. The contribution of E_{counter} , evaluated within the factorization model, is of the same order as $E_{\text{loop,subtracted}}$. For $K^+ \rightarrow \pi^0\pi^0\pi^+\gamma$ there is an almost complete destructive interference between loops and electric counterterms, while for $K^+ \rightarrow \pi^+\pi^+\pi^-\gamma$ we find $E_{\text{counter}} \simeq E_{\text{loop,subtracted}}$. Finally, in the K_L channel $E_{\text{loop,subtracted}}$ is bigger than E_{counter} for large E_γ . For small E_γ , the two amplitudes are comparable. Probably only large deviations from the naive expectation $k_f \sim \mathcal{O}(1)$ could be observed. Also the magnetic contribution is very much suppressed in these channels: the ratio $\Gamma_{\text{M}}/\Gamma_{\text{GB}}$ is typically smaller than 10^{-3} .

Interference effects between electric and magnetic amplitudes could in principle be larger. For instance, observables like $\det(p_1, p_2, p_3, p_4)$ (for the decays with three different pions in the final state) or $\nu \det(p_1, p_2, p_3, p_4)$ (in the case of two identical particles π_1, π_2) are sensitive

to such interferences. To $\mathcal{O}(p^4)$, the interference term

$$\varepsilon^{\mu\nu\rho\sigma}(E_\mu M_{\nu\rho\sigma}^* + E_\mu^* M_{\nu\rho\sigma}) \quad (5.1)$$

is proportional to the relatively small absorptive part of the electric amplitude. Thus, the leading-order piece of E_μ does not contribute in (5.1). Nevertheless, the possibility of interference measurements should be kept in mind once sufficiently high statistics will have been achieved.

For the three channels under consideration, the amplitude is completely dominated by generalized bremsstrahlung. In the last column of Tables 2 – 4, we therefore list the branching ratios based on generalized bremsstrahlung only, corresponding to Γ_{GB} in the second column. The contributions to the branching ratios from direct emission are completely concealed by the present experimental uncertainties of the $K \rightarrow 3\pi$ parameters.

Within those errors, our predictions are consistent with standard bremsstrahlung and with the available experimental results. Our theoretical branching ratio for $K^- \rightarrow \pi^0\pi^0\pi^-\gamma$ in Table 2 for $E_\gamma > 10\text{MeV}$ can be compared directly with the experimental result [1]

$$\text{BR}(K^- \rightarrow \pi^0\pi^0\pi^-\gamma) = (7.4_{-2.9}^{+5.5}) \cdot 10^{-6}, \quad E_\gamma > 10 \text{ MeV}. \quad (5.2)$$

For $K^+ \rightarrow \pi^+\pi^+\pi^-\gamma$, Barmin et al. [2] have reported the branching ratio

$$\text{BR}(K^+ \rightarrow \pi^+\pi^+\pi^-\gamma) = (1.10 \pm 0.48) \cdot 10^{-4}, \quad E_\gamma > 5 \text{ MeV}, \quad (5.3)$$

to be compared with our theoretical prediction

$$\text{BR}(K^+ \rightarrow \pi^+\pi^+\pi^-\gamma)|_{\text{theor.}} = (1.26 \pm 0.01) \cdot 10^{-4}, \quad E_\gamma > 5 \text{ MeV}, \quad (5.4)$$

whereas Stamer et al. [3, 26] have found

$$\text{BR}(K^+ \rightarrow \pi^+\pi^+\pi^-\gamma) = (1.0 \pm 0.4) \cdot 10^{-4}, \quad E_\gamma > 11 \text{ MeV}. \quad (5.5)$$

For the decay $K_S \rightarrow \pi^+\pi^-\pi^0\gamma$ the situation is quite different. To lowest chiral order, the amplitude can only proceed through a $\Delta I = 3/2$ transition (via bremsstrahlung) and is therefore suppressed by the $\Delta I = 1/2$ rule. Consequently, the next-to-leading order contributions generated by octet operators are becoming relatively more important⁴. At the one-loop level, two-pion intermediate states do not contribute. Therefore, the $\mathcal{O}(p^4)$ part of the electric amplitude is essentially determined by the counterterm

$$N_{K_S}(\mu) := [7(N_{14}^r - N_{16}^r) + 5(N_{15}^r + N_{17}^r)](\mu) \quad (5.6)$$

that is predicted to be large by the factorization model in (3.8). Its rather modest scale dependence,

$$N_{K_S}(\mu_2) = N_{K_S}(\mu_1) + \frac{3}{8\pi^2} \ln(\mu_1/\mu_2), \quad (5.7)$$

⁴A similar phenomenon occurs in the $K^+ \rightarrow \pi^+\pi^0\gamma$ decay [24, 27].

Table 2: Numerical results for the decay $K^+ \rightarrow \pi^0 \pi^0 \pi^+ \gamma$. The photon energy E_γ and the decay widths Γ_{GB} , Γ_{M} are given in MeV.

E_γ	Γ_{GB}	$\frac{\Gamma_{\text{GB}} - \Gamma_{\text{Low}}}{\Gamma}$	$\frac{\Gamma_{\text{E}} - \Gamma_{\text{GB}}}{\Gamma}$	Γ_{M}	BR
10–20	$(1.38 \pm 0.02) \cdot 10^{-19}$	$1.4 \cdot 10^{-3}$	$2.2 \cdot 10^{-5}$	$2.8 \cdot 10^{-25}$	$(2.60 \pm 0.03) \cdot 10^{-6}$
20–30	$(4.29 \pm 0.06) \cdot 10^{-20}$	$4.5 \cdot 10^{-3}$	$8.2 \cdot 10^{-5}$	$7.5 \cdot 10^{-25}$	$(8.05 \pm 0.01) \cdot 10^{-7}$
30–40	$(1.45 \pm 0.03) \cdot 10^{-20}$	$9.8 \cdot 10^{-3}$	$2.5 \cdot 10^{-4}$	$1.1 \cdot 10^{-24}$	$(2.72 \pm 0.05) \cdot 10^{-7}$
40–50	$(4.48 \pm 0.09) \cdot 10^{-21}$	$1.8 \cdot 10^{-2}$	$2.2 \cdot 10^{-4}$	$1.1 \cdot 10^{-24}$	$(8.42 \pm 0.18) \cdot 10^{-8}$
50–60	$(1.09 \pm 0.03) \cdot 10^{-21}$	$2.9 \cdot 10^{-2}$	$-1.0 \cdot 10^{-3}$	$6.8 \cdot 10^{-25}$	$(2.05 \pm 0.05) \cdot 10^{-8}$
60–70	$(1.49 \pm 0.05) \cdot 10^{-22}$	$4.3 \cdot 10^{-2}$	$-6.8 \cdot 10^{-3}$	$2.0 \cdot 10^{-25}$	$(2.81 \pm 0.09) \cdot 10^{-9}$
70–80	$(3.48 \pm 0.12) \cdot 10^{-24}$	$5.6 \cdot 10^{-2}$	$-1.9 \cdot 10^{-2}$	$8.9 \cdot 10^{-27}$	$(6.55 \pm 0.23) \cdot 10^{-11}$
10–80	$(2.01 \pm 0.03) \cdot 10^{-19}$	$3.3 \cdot 10^{-3}$	$4.5 \cdot 10^{-5}$	$4.1 \cdot 10^{-24}$	$(3.78 \pm 0.05) \cdot 10^{-6}$

Table 3: Numerical results for the decay $K^+ \rightarrow \pi^+ \pi^+ \pi^- \gamma$.

E_γ	Γ_{GB}	$\frac{\Gamma_{\text{GB}} - \Gamma_{\text{Low}}}{\Gamma}$	$\frac{\Gamma_{\text{E}} - \Gamma_{\text{GB}}}{\Gamma}$	Γ_{M}	BR
10–20	$(2.32 \pm 0.02) \cdot 10^{-18}$	$-1.7 \cdot 10^{-3}$	$-4.2 \cdot 10^{-4}$	$1.3 \cdot 10^{-24}$	$(4.36 \pm 0.04) \cdot 10^{-5}$
20–30	$(7.63 \pm 0.07) \cdot 10^{-19}$	$-4.8 \cdot 10^{-3}$	$-1.2 \cdot 10^{-3}$	$3.2 \cdot 10^{-24}$	$(1.43 \pm 0.01) \cdot 10^{-5}$
30–40	$(2.62 \pm 0.03) \cdot 10^{-19}$	$-9.2 \cdot 10^{-3}$	$-2.4 \cdot 10^{-3}$	$4.1 \cdot 10^{-24}$	$(4.93 \pm 0.05) \cdot 10^{-6}$
40–50	$(7.66 \pm 0.08) \cdot 10^{-20}$	$-1.5 \cdot 10^{-2}$	$-4.1 \cdot 10^{-3}$	$3.2 \cdot 10^{-24}$	$(1.44 \pm 0.01) \cdot 10^{-6}$
50–60	$(1.43 \pm 0.02) \cdot 10^{-20}$	$-2.1 \cdot 10^{-2}$	$-6.2 \cdot 10^{-3}$	$1.3 \cdot 10^{-24}$	$(2.69 \pm 0.03) \cdot 10^{-7}$
60–70	$(7.23 \pm 0.09) \cdot 10^{-22}$	$-2.8 \cdot 10^{-2}$	$-8.5 \cdot 10^{-3}$	$1.2 \cdot 10^{-25}$	$(1.36 \pm 0.02) \cdot 10^{-8}$
10–70	$(3.44 \pm 0.03) \cdot 10^{-18}$	$-3.4 \cdot 10^{-3}$	$-8.5 \cdot 10^{-4}$	$1.3 \cdot 10^{-23}$	$(6.46 \pm 0.06) \cdot 10^{-5}$

is compensated by loop graphs with kaon intermediate states which we have neglected. The uncertainty induced by this scale dependence,

$$\frac{N_{K_S}(0.5 \text{ GeV}) - N_{K_S}(1 \text{ GeV})}{N_{K_S}^{\text{FM}}} \simeq 0.09, \quad (5.8)$$

with $N_{K_S}^{\text{FM}}$ given by (3.8) for $k_f = 1$, is certainly smaller than the intrinsic uncertainty of the factorization hypothesis.

The corresponding numerical results are displayed in Table 5. The numbers for Γ_{E} are obtained from the sum of E_{GB} (using the central values of the input parameters b_2 and d_2 in (2.14)) and the aforementioned $\mathcal{O}(p^4)$ counterterm amplitude. Note that the interference is destructive and especially pronounced at large values of E_γ . The contribution of the magnetic amplitude is again shown for $a_i = 1$. For this channel we list the total branching ratio $\text{BR} = (\Gamma_{\text{E}} + \Gamma_{\text{M}})/\Gamma_{\text{tot}}(K_S)$ for the various photon energy bins. We do not give errors for these branching ratios because, unlike for the other three channels, the direct emission

Table 4: Numerical results for the decay $K_L \rightarrow \pi^+\pi^-\pi^0\gamma$.

E_γ	Γ_{GB}	$\frac{\Gamma_{\text{GB}} - \Gamma_{\text{Low}}}{\Gamma}$	$\frac{\Gamma_{\text{E}} - \Gamma_{\text{GB}}}{\Gamma}$	Γ_{M}	BR
10–20	$(1.32 \pm 0.02) \cdot 10^{-18}$	$-4.5 \cdot 10^{-3}$	$-4.2 \cdot 10^{-4}$	$2.1 \cdot 10^{-26}$	$(1.04 \pm 0.02) \cdot 10^{-4}$
20–30	$(4.89 \pm 0.07) \cdot 10^{-19}$	$-1.3 \cdot 10^{-2}$	$-1.1 \cdot 10^{-3}$	$4.4 \cdot 10^{-26}$	$(3.84 \pm 0.06) \cdot 10^{-5}$
30–40	$(1.98 \pm 0.03) \cdot 10^{-19}$	$-2.5 \cdot 10^{-2}$	$-1.8 \cdot 10^{-3}$	$5.0 \cdot 10^{-26}$	$(1.55 \pm 0.03) \cdot 10^{-5}$
40–50	$(7.33 \pm 0.11) \cdot 10^{-20}$	$-4.0 \cdot 10^{-2}$	$-1.7 \cdot 10^{-3}$	$3.7 \cdot 10^{-26}$	$(5.76 \pm 0.10) \cdot 10^{-6}$
50–60	$(2.13 \pm 0.04) \cdot 10^{-20}$	$-5.8 \cdot 10^{-2}$	$2.5 \cdot 10^{-3}$	$1.7 \cdot 10^{-26}$	$(1.67 \pm 0.03) \cdot 10^{-6}$
60–70	$(3.39 \pm 0.06) \cdot 10^{-21}$	$-7.9 \cdot 10^{-2}$	$2.7 \cdot 10^{-2}$	$3.5 \cdot 10^{-27}$	$(2.67 \pm 0.05) \cdot 10^{-7}$
70–80	$(8.04 \pm 0.15) \cdot 10^{-23}$	$-9.9 \cdot 10^{-2}$	$2.2 \cdot 10^{-1}$	$9.5 \cdot 10^{-29}$	$(6.32 \pm 0.13) \cdot 10^{-9}$
10–80	$(2.11 \pm 0.03) \cdot 10^{-18}$	$-1.0 \cdot 10^{-2}$	$-6.6 \cdot 10^{-4}$	$1.7 \cdot 10^{-25}$	$(1.65 \pm 0.03) \cdot 10^{-4}$

 Table 5: Numerical results for the decay $K_S \rightarrow \pi^+\pi^-\pi^0\gamma$.

E_γ	Γ_{GB}	$\frac{\Gamma_{\text{GB}} - \Gamma_{\text{Low}}}{\Gamma}$	Γ_{E}	Γ_{M}	BR
10–20	$(1.29 \pm 0.34) \cdot 10^{-21}$	$1.2 \cdot 10^{-2}$	$1.1 \cdot 10^{-21}$	$6.5 \cdot 10^{-25}$	$1.5 \cdot 10^{-10}$
20–30	$(5.15 \pm 1.28) \cdot 10^{-22}$	$3.8 \cdot 10^{-2}$	$3.4 \cdot 10^{-22}$	$1.6 \cdot 10^{-24}$	$4.7 \cdot 10^{-11}$
30–40	$(2.34 \pm 0.53) \cdot 10^{-22}$	$7.7 \cdot 10^{-2}$	$9.7 \cdot 10^{-23}$	$2.3 \cdot 10^{-24}$	$1.3 \cdot 10^{-11}$
40–50	$(9.97 \pm 2.12) \cdot 10^{-23}$	$1.2 \cdot 10^{-1}$	$2.0 \cdot 10^{-23}$	$2.1 \cdot 10^{-24}$	$2.9 \cdot 10^{-12}$
50–60	$(3.34 \pm 0.68) \cdot 10^{-23}$	$1.6 \cdot 10^{-1}$	$2.2 \cdot 10^{-24}$	$1.2 \cdot 10^{-24}$	$4.6 \cdot 10^{-13}$
60–70	$(6.09 \pm 1.22) \cdot 10^{-24}$	$2.1 \cdot 10^{-1}$	$2.3 \cdot 10^{-25}$	$3.4 \cdot 10^{-25}$	$7.8 \cdot 10^{-14}$
70–80	$(1.62 \pm 0.32) \cdot 10^{-25}$	$2.4 \cdot 10^{-1}$	$1.7 \cdot 10^{-26}$	$1.2 \cdot 10^{-26}$	$4.0 \cdot 10^{-15}$
10–80	$(2.18 \pm 0.55) \cdot 10^{-21}$	$3.3 \cdot 10^{-2}$	$1.6 \cdot 10^{-21}$	$8.2 \cdot 10^{-24}$	$2.2 \cdot 10^{-10}$

amplitude matters with unknown theoretical uncertainties (factorization model).

Remembering the projected DAΦNE yield of $7.5 \times 10^9 K_L K_S$ pairs per year, the $K_S \rightarrow \pi^+\pi^-\pi^0\gamma$ decay rate is still too small for the coming generation of kaon experiments. With an additional improvement of statistics, some information might be achieved via time–interference measurements [28] ($K_{L,S} \rightarrow \pi^+\pi^-\pi^0\gamma$) similar to those recently performed in the non–radiative case [29, 30]. Then interference effects between electric and magnetic amplitudes could in principle be measured since a term like

$$\varepsilon^{\mu\nu\rho\sigma}(E_\mu M_{\nu\rho\sigma}^* - E_\mu^* M_{\nu\rho\sigma}) \quad (5.9)$$

is generated. In contrast to (5.1), this term is proportional to the leading–order piece of E_μ . We stress that even fixed–target experiments, through regeneration, can perform time–interference measurements and in this case a larger statistics is expected. Thus, the $K_S \rightarrow \pi^+\pi^-\pi^0\gamma$ decay mode may still turn out to be a valuable probe for kaon physics parameters that is not drowned by bremsstrahlung.

6 Conclusions

Anticipating substantial improvements in the statistics of $K \rightarrow 3\pi\gamma$ decays in the near future, we have performed a comprehensive and complete analysis of these decays to $\mathcal{O}(p^4)$ in the low-energy expansion of the Standard Model. To lowest order, $\mathcal{O}(p^2)$, the decay amplitudes are determined by the corresponding non-radiative amplitudes via Low's theorem (bremsstrahlung). At next-to-leading order, there are different contributions to both electric and magnetic parts of the amplitudes: loops and tree-level (counterterm) amplitudes, reducible and irreducible contributions.

A major aspect of our analysis is the concept of “generalized bremsstrahlung” that transfers the available theoretical or experimental information on $K \rightarrow 3\pi$ decays to the corresponding radiative amplitudes in an optimal way at the level of $\mathcal{O}(p^4)$. For the numerical analysis, we have used the factorization hypothesis to estimate the relevant low-energy constants.

Returning to the three issues addressed in the introduction, we may summarize our findings as follows:

- i. In all three channels where the leading-order amplitudes are not suppressed ($K^+ \rightarrow \pi^0\pi^0\pi^+\gamma$, $K^+ \rightarrow \pi^+\pi^+\pi^-\gamma$, $K_L \rightarrow \pi^+\pi^-\pi^0\gamma$), generalized bremsstrahlung completely dominates the amplitudes to $\mathcal{O}(p^4)$. The differences to the QED prediction (standard or internal bremsstrahlung) could be experimentally observed in the forthcoming round of kaon experiments, at least from the statistical point of view.
- ii. For the same channels, it will hardly be possible to extract the appropriate combinations of low-energy constants from experiment in the near future. This conclusion hinges, of course, on the assumption that the factorization estimates are not off by an order-of-magnitude in amplitude. In contrast, the counterterm amplitude is important for $K_S \rightarrow \pi^+\pi^-\pi^0\gamma$, especially if the rather large factorization estimate is reliable. However, for this decay mode the branching ratio is probably too small to be detected soon.
- iii. As a general conclusion, the Standard Model allows for quite definite predictions for radiative kaon decays into three pions. Especially for $K^+ \rightarrow \pi^0\pi^0\pi^+\gamma$, $K^+ \rightarrow \pi^+\pi^+\pi^-\gamma$ and $K_L \rightarrow \pi^+\pi^-\pi^0\gamma$, the accuracy of these predictions is at the moment only limited by the precision with which the parameters of the non-radiative decay amplitudes are known. For $K_S \rightarrow \pi^+\pi^-\pi^0\gamma$, there is some theoretical uncertainty related to the relevant low-energy constants.

As soon as more accurate data will lead to better precision for the $K \rightarrow 3\pi$ parameters, the predictions of the radiative amplitudes can be improved accordingly. Although we have only considered total rates and photon energy spectra in this analysis, the investigation of more subtle effects like the interference between electric and magnetic amplitudes may then become feasible.

Acknowledgements

One of us (G. D'A.) wants to thank F. Sannino for discussions.

Appendix: Loop amplitudes

In this Appendix, we collect the main results of Ref. [7] for the calculation of loop amplitudes corresponding to the diagram in Fig. 1.

First, we calculate the loop amplitude for the non-radiative process $K \rightarrow 3\pi$. In our case, $-p_a = -p_4$ is the kaon momentum and V_1, V_2 are nonleptonic weak and strong vertices, respectively. The pion momenta are generically denoted p_b, p_c, p_d .

We characterize the vertices V_1, V_2 in momentum space by constants a_i, b_i :

$$\begin{aligned} V_1 &= a_0 + a_1 p_a \cdot p_b + a_2 p_a \cdot x + a_3(x^2 - M_x^2) + a_4(y^2 - M_y^2) + a_5(p_a^2 - M_a^2) + a_6(p_b^2 - M_b^2) \\ V_2 &= b_0 + b_1 p_c \cdot p_d + b_2 p_c \cdot x + b_3(x^2 - M_x^2) + b_4(y^2 - M_y^2) + b_5(p_c^2 - M_c^2) + b_6(p_d^2 - M_d^2) . \end{aligned} \quad (\text{A.1})$$

With $P = p_c + p_d$, the non-radiative loop amplitude of Fig. 1 can be represented in the following form (all external lines are on-shell):

$$\begin{aligned} F(P) &= A(M_x)[a_1 b_4 p_a \cdot p_b + a_4 b_1 p_c \cdot p_d + a_4 b_4(P^2 + M_x^2 - M_y^2) + a_0 b_4 + a_4 b_0] \\ &\quad + A(M_y)[a_1 b_3 p_a \cdot p_b + a_2 b_3 p_a \cdot P + a_3 b_1 p_c \cdot p_d + a_3 b_2 p_c \cdot P \\ &\quad\quad + a_3 b_3(P^2 - M_x^2 + M_y^2) + a_0 b_3 + a_3 b_0] \\ &\quad + B(P^2, M_x, M_y)[a_0 b_0 + a_0 b_1 p_c \cdot p_d + a_1 b_0 p_a \cdot p_b + a_1 b_1 p_a \cdot p_b p_c \cdot p_d] \\ &\quad + B_1(P^2, M_x, M_y)[a_0 b_2 p_c \cdot P + a_2 b_0 p_a \cdot P + a_1 b_2 p_a \cdot p_b p_c \cdot P + a_2 b_1 p_c \cdot p_d p_a \cdot P] \\ &\quad + a_2 b_2 [p_a \cdot p_c B_{20}(P^2, M_x, M_y) + p_a \cdot P p_c \cdot P B_{22}(P^2, M_x, M_y)] . \end{aligned} \quad (\text{A.2})$$

The various functions in (A.2) are as defined conventionally (in d dimensions):

$$\begin{aligned} A(M) &= \frac{1}{i} \int \frac{d^d x}{(2\pi)^d} \frac{1}{x^2 - M^2} \\ (B, B_1 P_\mu, g_{\mu\nu} B_{20} + P_\mu P_\nu B_{22}) &= \frac{1}{i} \int \frac{d^d x}{(2\pi)^d} \frac{(1, x_\mu, x_\mu x_\nu)}{(x^2 - M_x^2)[(x - P)^2 - M_y^2]} . \end{aligned} \quad (\text{A.3})$$

We have chosen to express $F(P)$ in terms of the scalar products

$$p_a \cdot p_b, \quad p_c \cdot p_d, \quad P^2, \quad p_a \cdot P, \quad p_c \cdot P, \quad p_a \cdot p_c \quad (\text{A.4})$$

instead of using kinematical relations to express all scalar products in terms of the two independent scalar variables s, ν . Note that the analytically non-trivial part of (A.2), involving the various B functions, contains only the on-shell couplings $a_0, a_1, a_2, b_0, b_1, b_2$. The off-shell couplings a_3, a_4, b_3, b_4 appear only together with the divergent constants $A(M)$. Since these terms are polynomials in the momenta of at most degree two, they will enter in the radiative

Table 6: Coefficients of the vertices V_1, V_2 defined in (A.1) for the various loop diagrams. Only the relevant on-shell coefficients are listed.

$K(-p_a) \rightarrow \pi(p_b) + \pi(x)\pi(y) \rightarrow \pi(p_c)\pi(p_d)$	a_0	a_1	a_2	b_0	b_1	b_2
$K^+ \rightarrow \pi^+ + \pi^+\pi^- \rightarrow \pi^+\pi^-$	$-2M_K^2$	-2	-2	$2M_\pi^2$	2	-2
$K^+ \rightarrow \pi^+ + \pi^+\pi^- \rightarrow \pi^0\pi^0$	$-2M_K^2$	-2	-2	M_π^2	2	0
$K^+ \rightarrow \pi^+ + \pi^0\pi^0 \rightarrow \pi^+\pi^-$	$-M_K^2$	-2	0	M_π^2	2	0
$K^+ \rightarrow \pi^- + \pi^+\pi^+ \rightarrow \pi^+\pi^+$	0	2	0	0	-2	0
$K^+ \rightarrow \pi^0 + \pi^+\pi^0 \rightarrow \pi^+\pi^0$	$-M_K^2$	0	-2	M_π^2	0	-2
$K^0 \rightarrow \pi^+ + \pi^0\pi^- \rightarrow \pi^0\pi^-$	$M_K^2/\sqrt{2}$	0	$\sqrt{2}$	M_π^2	0	-2
$K^0 \rightarrow \pi^- + \pi^0\pi^+ \rightarrow \pi^0\pi^+$	$M_K^2/\sqrt{2}$	0	$\sqrt{2}$	M_π^2	0	-2
$K^0 \rightarrow \pi^0 + \pi^+\pi^- \rightarrow \pi^+\pi^-$	$M_K^2/\sqrt{2}$	$\sqrt{2}$	0	$2M_\pi^2$	2	-2

amplitude only through internal bremsstrahlung and will therefore eventually be absorbed in E_{GB}^μ . The on-shell coefficients for the various channels are listed in Table 6.

We now turn to the radiative loop amplitude and decompose it into two parts:

$$E_{\text{loop}}^\mu = G^\mu + H^\mu. \quad (\text{A.5})$$

The amplitude G^μ can be expressed through derivatives of the non-radiative loop amplitude F in (A.2) with respect to the various scalar products (A.4). In some of the following terms, the momentum P has to be replaced by $P + k$, leaving all scalar products unchanged that do not contain P explicitly:

$$\begin{aligned}
G^\mu = & F(P)\Sigma^\mu + \frac{F(P+k) - F(P)}{k \cdot P} \Lambda_{cd}^\mu + \frac{\partial F}{\partial(p_a \cdot p_b)}(P) \Lambda_{ab}^\mu \\
& + \frac{\partial F}{\partial(p_a \cdot P)}(P) \Lambda_{aP}^\mu + \frac{\partial F}{\partial(p_c \cdot p_d)}(P+k) \Lambda_{cd}^\mu + \frac{\partial F}{\partial(p_c \cdot P)}(P+k) \Lambda_{cP}^\mu \\
& + \left[q_a t_c \frac{\partial F}{\partial(p_a \cdot p_c)}(P) - q_c t_a \frac{\partial F}{\partial(p_a \cdot p_c)}(P+k) \right] D_{ac}^\mu \\
& - \frac{1}{2} (q_c + q_d) t_a t_c \left[\frac{\partial^2 F}{\partial(p_a \cdot P) \partial(p_c \cdot P)}(P) D_{aP}^\mu - \frac{\partial^2 F}{\partial(p_a \cdot P) \partial(p_c \cdot P)}(P+k) D_{cP}^\mu \right].
\end{aligned} \quad (\text{A.6})$$

We have used the definitions (2.9). When P appears as an index (e.g., in Λ_{aP}^μ or D_{cP}^μ), the corresponding momentum and charge in (2.9) are P and $q_c + q_d$, respectively.

The second part H^μ of the loop amplitude (A.5) cannot be expressed in terms of F or derivatives thereof. For the relevant case of equal loop masses ($M_x = M_y = M_\pi =: M$), H^μ takes on the following compact form:

$$\begin{aligned}
H^\mu = & a_2(t_b p_a^\mu - t_a p_b^\mu) \{ (q_x - q_y) (2b_0 + 2b_1 p_c \cdot p_d + b_2 p_c \cdot P) \widetilde{C}_{20}(P^2, -k \cdot P) \\
& + b_2 (q_x + q_y) [-2p_c \cdot P \widetilde{C}_{31}(P^2, -k \cdot P) + 2t_c \widetilde{C}_{32}(P^2, -k \cdot P) - p_c \cdot P \widetilde{C}_{20}(P^2, -k \cdot P)] \} \\
& + b_2 (t_d p_c^\mu - t_c p_d^\mu) \{ (q_x - q_y) [2a_0 + 2a_1 p_a \cdot p_b + a_2 (p_a \cdot P + t_a)] \widetilde{C}_{20}((P+k)^2, k \cdot P) \\
& + a_2 (q_x + q_y) [-2(p_a \cdot P + t_a) \widetilde{C}_{31}((P+k)^2, k \cdot P) - 2t_a \widetilde{C}_{32}((P+k)^2, k \cdot P) \\
& - (p_a \cdot P + t_a) \widetilde{C}_{20}((P+k)^2, k \cdot P)] \} . \tag{A.7}
\end{aligned}$$

The functions \widetilde{C}_{ij} are defined as

$$\widetilde{C}_{ij}(u, v) = \frac{C_{ij}(u, v) - C_{ij}(u, 0)}{v} \tag{A.8}$$

in terms of the three-propagator one-loop functions $C_{ij}(p^2, k \cdot p)$ for $k^2 = 0$:

$$\begin{aligned}
& \frac{1}{i} \int \frac{d^d x}{(2\pi)^d} \frac{\{x_\mu x_\nu, x_\mu x_\nu x_\rho\}}{(x^2 - M^2)[(x+p)^2 - M^2][(x+k)^2 - M^2]} = \\
& = \{C_{20}(p^2, k \cdot p) g_{\mu\nu} + \dots, C_{31}(p^2, k \cdot p) (p_\mu g_{\nu\rho} + p_\nu g_{\mu\rho} + p_\rho g_{\mu\nu}) \\
& \quad + C_{32}(p^2, k \cdot p) (k_\mu g_{\nu\rho} + k_\nu g_{\mu\rho} + k_\rho g_{\mu\nu}) + \dots\} . \tag{A.9}
\end{aligned}$$

We recall the following observations from Ref. [7]:

- i. The amplitudes G^μ in (A.6) and H^μ in (A.7) are separately gauge invariant.
- ii. The amplitude H^μ is finite and at least of $\mathcal{O}(k)$. It only contains the on-shell couplings $a_0, a_1, a_2, b_0, b_1, b_2$ defined in (A.1) and the charges q_x, q_y of the particles in the loop.
- iii. The generalized bremsstrahlung part of the loop amplitude is contained in G^μ . Denoting by $E_{\text{GB}}^\mu(\text{loop})$ the result obtained by inserting for $A(s, \nu)$ the on-shell loop amplitude (A.2) in Eq. (2.11), the difference

$$\Delta^\mu = G^\mu - E_{\text{GB}}^\mu(\text{loop}) \tag{A.10}$$

is at least of $\mathcal{O}(k)$. Moreover, by construction of E_{GB}^μ all the divergences in Δ^μ are renormalized by counterterms with an explicit field strength tensor. Finally, Δ^μ is finite for $a_2 b_2 = 0$.

Putting everything together, the subtracted loop amplitude $E_{\text{loop,subtracted}}^\mu$ in (3.1) is given by

$$E_{\text{loop,subtracted}}^\mu = \sum_{\text{loops}} (\Delta^\mu + H^\mu) . \tag{A.11}$$

The sum extends over the various configurations listed in Table 6.

References

- [1] V.N. Bolotov et al., J. Exp. Th. Phys. Lett. 42 (1985) 481.
- [2] V.V. Barmin et al., Sov. J. Nucl. Phys. 50 (1989) 421.
- [3] P. Stamer et al., Phys. Rev. 138B (1965) 440.
- [4] The Second DAΦNE Physics Handbook, Eds. L. Maiani, G. Pancheri and N. Paver (Servizio Documentazione INFN, Frascati, 1995).
- [5] Proceedings of the Workshop on K Physics, Orsay, France, May 30 – June 4, 1996; Proceedings of the Workshop on Heavy Quarks at Fixed Target, Rheinfels Castle, St. Goar, Germany, Oct. 3 – 6, 1996.
- [6] S. Weinberg, Physica 96A (1979) 327;
J. Gasser and H. Leutwyler, Ann. Phys. (N.Y.) 158 (1984) 142; Nucl. Phys. B250 (1985) 465;
H. Leutwyler, Ann. Phys. (N.Y.) 235 (1994) 165.
- [7] G. D'Ambrosio, G. Ecker, G. Isidori and H. Neufeld, Phys. Lett. B380 (1996) 165.
- [8] G. D'Ambrosio, G. Ecker, G. Isidori and H. Neufeld, Radiative nonleptonic kaon decays, in: Ref. [4], p. 265.
- [9] J. Kambor, J. Missimer and D. Wyler, Nucl. Phys. B346 (1990) 17.
- [10] G. Ecker, J. Kambor and D. Wyler, Nucl. Phys. B394 (1993) 101.
- [11] F.E. Low, Phys. Rev. 110 (1958) 974.
- [12] J. Wess and B. Zumino, Phys. Lett. 37B (1971) 95;
E. Witten, Nucl. Phys. B223 (1983) 422.
- [13] G. Ecker, A. Pich and E. de Rafael, Phys. Lett. B189 (1987) 363; Nucl. Phys. B303 (1988) 665.
- [14] R.H. Dalitz, Phys. Rev. 99 (1955) 915.
- [15] G. D'Ambrosio, M. Miragliuolo and P. Santorelli, Radiative nonleptonic kaon decays, in The DAΦNE Physics Handbook, Eds. L. Maiani, G. Pancheri and N. Paver (Servizio Documentazione INFN, Frascati, 1992).
- [16] F. Sannino, Tesi di Laurea, Università di Napoli Federico II (1992).
- [17] R. Ferrari and M. Rosa-Clot, Nuovo Cimento LVI (1968) 582.
- [18] T.J. Devlin and J.O. Dickey, Rev. Mod. Phys. 51 (1979) 237.
- [19] J. Kambor, J. Missimer and D. Wyler, Phys. Lett. B261 (1991) 496.

- [20] G. D'Ambrosio, G. Isidori, A. Pugliese and N. Paver, Phys. Rev. D50 (1994) 5767.
- [21] L. Maiani and N. Paver, CP conserving nonleptonic $K \rightarrow 3\pi$ decays, in: Ref. [4], p. 239.
- [22] V.Y. Batusov et al. (Serpukhov-167 Collaboration), Measurement of Dalitz-plot slope parameters for $K^+ \rightarrow \pi^+\pi^0\pi^0$ decay, talk presented by N. Russakovich at ICHEP '96 (Warsaw 1996).
- [23] G. Ecker, H. Neufeld and A. Pich, Phys. Lett. B278 (1992) 337.
- [24] G. Ecker, H. Neufeld and A. Pich, Nucl. Phys. B413 (1994) 321.
- [25] J. Bijnens, G. Ecker and A. Pich, Phys. Lett. B286 (1992) 341.
- [26] Particle Data Group, Phys. Rev. D54 (1996) Number 1, Part I.
- [27] G. D'Ambrosio and G. Isidori, Z. Phys. C65 (1996) 649.
- [28] G. D'Ambrosio and N. Paver, Phys. Rev. D46 (1992) 352; *ibid.* D49 (1994) 4560.
- [29] G.B. Thomson et al., Phys. Lett. B337 (1994) 411.
- [30] R. Adler et al. (CPLEAR Collaboration), Phys. Lett. B374 (1996) 313.